



Calibration and validation of WD-XRF multielement
method as well as standardized methods ASTM
D2622/4927 and ISO 20884

Student name: Rik van Tilborg
Student number: 00071132
HZ supervisor: Geert Mol
Company supervisor: Roeland Makkee
Date: 05/06/2020
Version: 1

Abstract

In this research several methods were developed and validated using the Supermini 200 wavelength dispersive X-ray fluorescence spectrometer. A multielement was calibrated containing 26 elements and corrected for interference according to the de Jongh algorithm. The limits of detection and quantification as well as the reproducibility show variation depending on element mass and the characteristic X-ray used for measurements. Detection of low concentration (10ppm) for light elements was shown to be impossible and for elements silver to bismuth large variations were found. Two standardized methods namely the ASTM D2622 and ISO 20884 were successfully calibrated and validated such that the repeatability and reproducibility were below that of the method after compensating for the fact that these were measured in a single laboratory on one machine. The calibration of ASTM D4927 was attempted but due to solubility issues it was unable to be calibrated and validated. It was found that helium could be saved by measuring the pulse height adjustment less frequently. Future research should determine the repeatability of the multielement method as well as the calibration and validation of ASTM D4927 and other standardized methods.

Abbreviations

SGS	Societe Generale de Surveillance
WD-XRF	wavelength dispersive x-ray fluorescence
ASTM	ASTM International, formerly American Society for Testing and Materials
ISO	International Organization for Standardization
m/m%	mass/mass%
P10 gas	A gas mixture of 90% Ar and 10% methane
PHA	Pulse height adjustment
PC	Proportional counter
SC	Scintillation counter
μm	micrometer
XRF	X-ray fluorescence

Contents

Abstract.....	1
Abbreviations.....	2
Introduction	5
Theoretical framework	6
X-ray fluorescence	6
X-ray source	6
Sample irradiation.....	7
Compton and Rayleigh scattering.....	8
Wavelength dispersive X-ray fluorescence.....	9
Diffractive crystals.....	9
Detection.....	10
Matrix effect	10
Interference correction.....	10
Materials and Methods.....	12
Materials	12
Chemicals	12
Methods.....	12
Method development.....	13
Multielement	16
ASTM D2622.....	17
ISO 20884	17
Results and Discussion	18
Multielement method.....	18
ASTM D 2622.....	21
ASTM D4927.....	23
ISO 20884	23
Conclusion.....	25
Recommendations	26
Bibliography	27
Appendix	28
I.	28
II, Validation ASTM D2622	28

III, Validation ISO 20884..... 30

Introduction

The International Maritime Organization, an agency backed by the United Nations, is the “global standard-setting authority for the safety, security and environmental performance of international shipping” (U.S. Energy Information Administration, 2019). This regulatory body is involved in reducing the amount of sulfur oxides (SO_x) being emitted from shipping. In addition to causing acid rain when these oxides mix with water in the atmosphere, they also cause health complications to living organisms (Agency for Toxic Substances and Disease Registry, 1999). As of the first of January 2020, a new regulation regarding the sulfur content of ship fuel has come into effect. The permitted amount has been decreased from 3.5%(m/m) to 0.5%(m/m) (U.S. Energy Information Administration, 2019). To ensure that the fuel abides by these new regulations, it must be tested after the production process.

SGS is a globally renowned independent inspection, verification, testing, and certifying company. At the Oil, Gas and Chemicals laboratory of SGS, in Spijkennise in the Netherlands, various departments carry out quality control analysis on a range of different samples. The petroleum department analyzes products such as fuel oils, lubricants, and other petroleum-based products to quantify elements and compounds of interest. A commonly requested analysis is that of heavy metals and or sulfur in organic compounds.

Heavy metals and sulfur can be determined in several organic matrices using wavelength dispersive X-ray fluorescence spectroscopy (WD-XRF). This approach is commonly used to detect sulfur in fuel, as well as metals and sulfur in lubricants and additives. This method of quantification allows for high elemental selectivity as well as broad elemental composition scans through the use of a moving detector combined with element-specific diffractive crystals. By applying internationally approved standardized methods together with this form of quantification, the results will be highly accurate, repeatable, and precise.

In this study intends sulfur concentrations were determined using a newly purchased WD-XRF manufactured by Rigaku. In order to satisfy the needs of the customers, the machine must run standard methods ASTM D2622/D4927 as well as ISO 20884 and uphold the stringent error margins described in each method. Furthermore, a quantitative method for the analysis of 26 elements in oil was developed and calibrated.

This research will seek to answer the questions listed below, as well as provide recommendations to expand the amount of standardized analysis done using WD-XRF.

1. Questions

- 1.1. Is it possible to correct for a complex multielement matrix?
 - 1.1.1. To what extent is this method accurate?
- 1.2. To what extent can sulfur be quantitatively measured using the Rigaku SuperMini 200 WD-XRF coupled with the RX9 crystal according to the ASTM D 2622 and ISO 20884 methods?
 - 1.2.1. What is the repeatability, reproducibility, limit of detection, and limit of quantification for these methods?
- 1.3. Is it possible to reduce the helium use of the Supermini 200?

Theoretical framework

X-ray fluorescence

X-ray fluorescence spectroscopy is a “fast, non-destructive and environmentally friendly analysis method which can be applied to measure both qualitatively and quantitatively” (Bruker AXS, 2000). According to the manufacturers of the SuperMini 200, Rigaku, it is possible to measure “solids, liquids, alloys, powders and thin films” with this technique. Furthermore, the use of Bohr’s model of the atom to classify elements based on their X-ray fluorescence allows versatility in that both single elements can be measured as well as a scan of all detectable elements to determine the chemical composition of the sample (Brouwer, 2003) (Bruker AXS, 2000).

X-ray source

Before an atom will fluoresce, it needs sufficient energy to remove an electron from one of the inner shells (Bertin, 1978). This is achieved by an end window X-ray source. Under a vacuum or helium atmosphere, the cathode is heated by applying a current to it, resulting in the release of electrons. Concurrently, a high positive voltage is applied to the anode, causing the electrons to accelerate towards it. These accelerated electrons will either slowdown in the electric field of an atomic orbital releasing Bremsstrahlung, or, if the energy is larger than the binding energy, which is the energy required to remove an electron from its shell, of the anode, they can cause the ejection of an inner-shell electron releasing element characteristic X-rays (Kramar, 1999). The Supermini 200 contains a palladium anode meaning that the characteristic X-rays of palladium will be present in all samples. Bremsstrahlung is a continuous spectrum in which X-rays of all energies ranging from 0 to the voltage applied to the anode are released. In the case of the Supermini 200, the voltage applied to the anode is 50 keV allowing all binding energies that fall within this range to be overcome and cause these elements to release characteristic X-rays. (Bruker AXS, 2000).

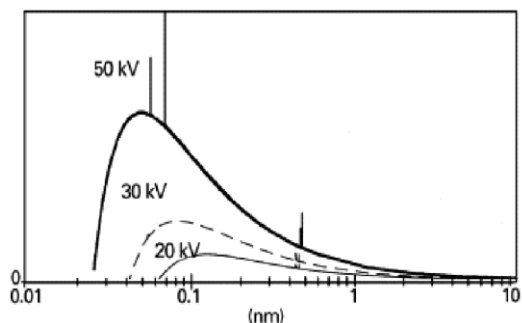


Figure 1: Example of Bremsstrahlung and characteristic anode line (Kramar, 1999)

Figure 1 shows the continuous source of X-rays from Bremsstrahlung as well as characteristic anode lines which are present by the large horizontal lines. It can be observed that depending on the voltage applied to the anode, the Bremsstrahlung changes as it is a distribution of X-rays released from the anode ranging from 0 to the voltage applied to the anode.

Sample irradiation

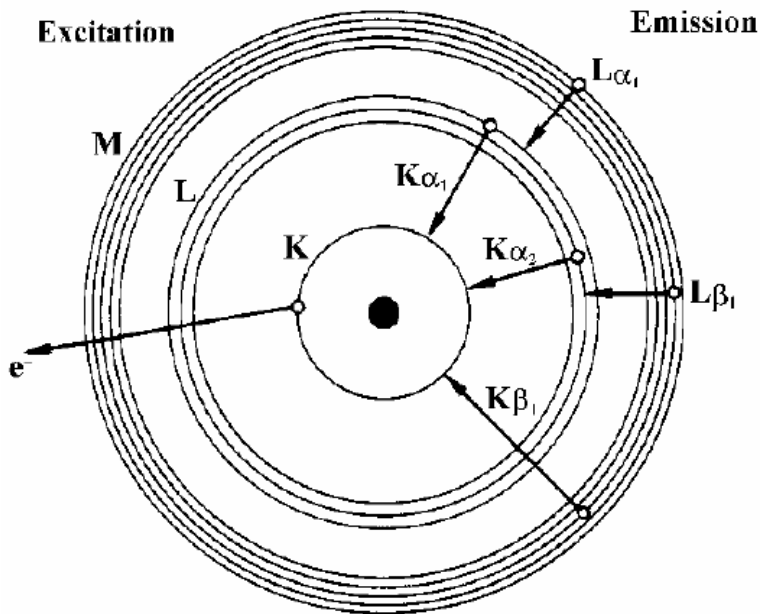
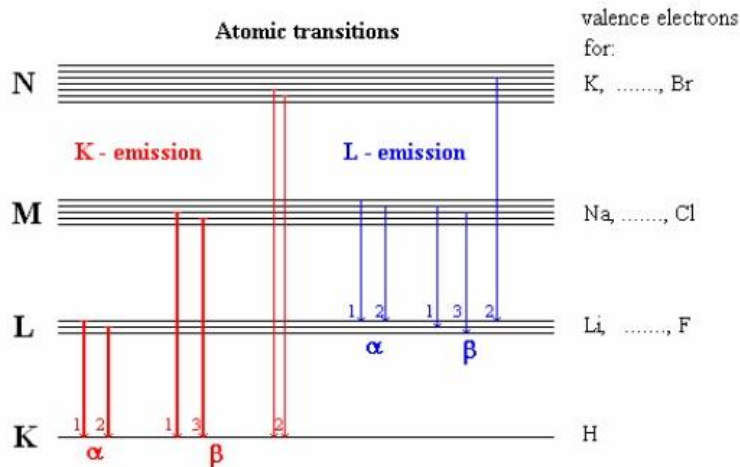


Figure 2: Bohr model of the atom (Bruker AXS, 2000)

As can be seen in figure 2, the Bohr model of the atom has different energy shells (K, L, M). Each shell contains electrons that are further divided into different subshells. The K shell contains 2 electrons that occupy one subshell. The L shell has 3 subshells that can contain up to 8 electrons. The M shell has 5 subshells that can contain a total of 18 electrons. When a sample is placed in a sample cup, with a transparent window at the bottom, and subsequently irradiated with X-rays, this results in the expulsion of an electron from an inner electron shell. The void left is filled by an electron from a higher energy shell and energy equal to the energy difference between the shells is released. This can then be detected, and a spectrum of all or specific elements present in the sample can be made. The machine looks for one specific or a mix of different emitted energies. As shown in figure 1, when an electron is emitted from the K shell, different electrons can fill the void, and each kind of radiation has its own name. (Brouwer, 2003) (Bruker AXS, 2000)



Examples:

- $K\alpha_1$ Electron from sub-level L_{III} to the K-shell
- $K\alpha_2$ Electron from sublevel L_{II} to the K-shell
- $K\alpha_{1,2}$ if neither line is resolved by the spectrometer
- $K\beta_1$ Electron from sublevel M to the K-shell
- $L\alpha_1$ Electron from sublevel M to the L-shell

Figure 3: Nomenclature of different drop energies (Bruker AXS, 2000)

As shown in figure 3, there are 2 different types of K and L radiation (α , β). Each of these is subsequently divided from highest energy difference to lowest. Each orbital has a specific binding energy. Due to differences in proton and electron number among the elements, the orbital specific energies vary allowing for quantification (Reichwein & Burgess, 2014).

Compton and Rayleigh scattering

Similarly to how inner-electrons are knocked out of their shell, Compton scattering is also an interaction between an X-ray and an electron. However, despite the energy of the X-ray far exceeding that of the binding energy, the result is not an electron being ejected from the atom. Instead, in Compton scattering the X-ray is deflected in a manner dependent on the incident angle. During this collision, the X-ray loses energy proportional to the incident angle, i.e., a low incident angle means the photon loses less energy, and an incident angle of 180° means the photon is backscattered and loses most of its energy. The effect Compton scattering has on measurements occurs via extra source peaks that are shifted slightly to the lower energy side of the spectrum. These peaks should always be in the same place because they are proportional to the angle at which the source irradiates the sample and because the source and sample compartment are fixed in XRF spectrometers. Due to this, the Compton scattering is the same in all measurements. (Simon R. Cherry, 2012)

Contrary to Compton scattering, Rayleigh scattering occurs when the X-rays are deflected without losing energy. This results in the X-rays from the source directly making it to the detector and therefore appearing in the spectrum even if there is none in the sample. When trying to determine if the source

material is in the sample, the source beam must then be passed through a primary beam filter, which absorbs the characteristic X-rays from the source material.

Wavelength dispersive X-ray fluorescence

As the name suggests, WD-XRF detects the specific wavelengths of the characteristic X-rays by using several components such as Soller slits and diffractive crystals. The purpose of the Soller slits, depicted below in figure 4, are to collimate all X-rays that are not travelling parallel to each other (Bertin, 1978). When a sample is irradiated, the fluorescent X-rays will travel in all directions. The Soller slits are made such that the incoming radiation is scattered to form a parallel beam, which can then be diffracted using crystals.

Diffractive crystals

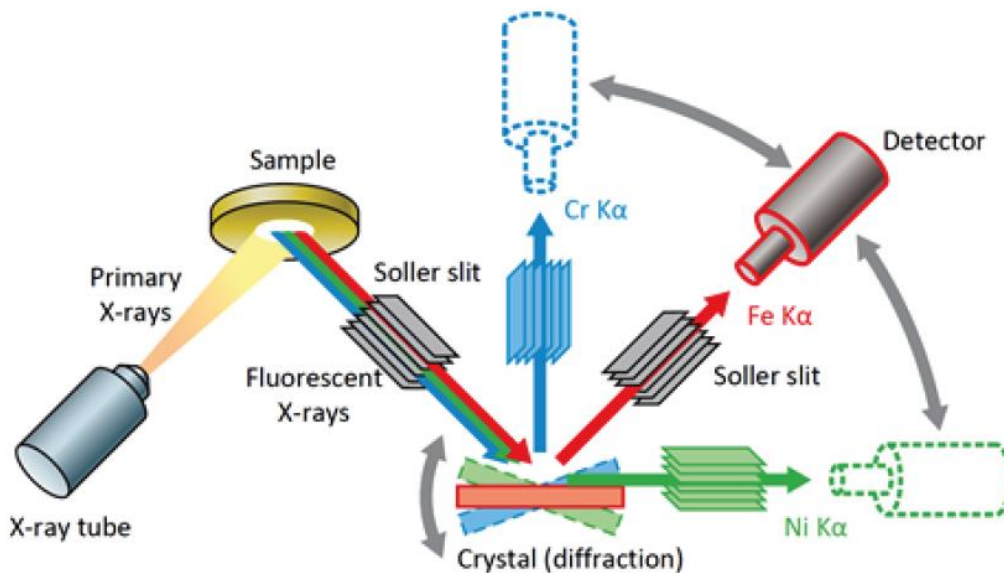


Figure 4: Optical configuration of Supermini 200 (Rigaku)

Figure 4 shows the way the Supermini 200 uses refraction to measure different wavelengths. Depending on the material and orientation of these crystals, the incoming X-rays are diffracted to the detector. This allows the machine to separate background radiation from the X-ray source as well as non-desired wavelengths from the desired wavelength, thus reducing noise and spectral overlap. This is achieved through Bragg's law, which states that the wavelength (λ) can be calculated if the following are known: the incident angle of the electromagnetic radiation (θ), the planar distance (d) of a diffractive crystal and the order of reflection. The equation for Bragg's law can be found in Appendix I (Chatterjee, 2001). As the X-rays strike the crystal they are diffracted. Depending on the orientation and planar distance, certain wavelengths of light will be intensified through constructive interference. This means that when the wrong crystal is used, the planar distance will cause the waves to be diffracted at the wrong angle, and therefore they will no longer be in-phase, leading to a decrease in signal. This principle is responsible for the high accuracy measuring possible with WD-XRF. The SuperMini 200 contains three element-specific crystals. The RX9 crystal is specific for phosphorus, sulfur, chlorine, potassium, and calcium due to the planar distance allowing for constructive interference of X-rays specific to these elements depending on

its orientation (Chatterjee, 2001). The machine has two other crystals: the LiF (200), which is specific for elements between titanium and uranium, and the RX26 for elements between oxygen and silicon.

Detection

The Supermini 200 contains a proportional counter (PC) and a scintillation counter (SC) to detect the characteristic X-rays emitted by elements. In a PC, the X-ray ionizes the argon in P10 gas, creating an Ar⁺ ion and an e⁻ also known as an ion pair. Inside the detector there is an anode wire which attracts the electrons, accelerating them and causing the formations of more ion pairs. The ratio between detected ion pairs and initial ion pairs is directly proportional to the energy of the X-ray. The methane portion of the P10 gas stops the recombination of the ion with an electron. The PC detector contains a very thin window through which the incident X-rays travel. Due to this thin window low energy X-rays emitted by light elements can be detected (Bertin, 1978) (Bruker AXS, 2000)

In an SC detector, incident X-rays interact with a sodium iodide which, is enhanced with thallium, crystal causing it to scintillate and release light photons. These photons are amplified in a photomultiplier tube where this amplified light strikes a photodiode and is converted into an electrical signal. Similarly to the PC detector, the ratio between the initial light output and the amplified signal is directly proportional to the energy of the incident X-ray (Potts, 2005). Contrary to the PC detector, the SC detector has a beryllium window that absorbs low energy X-rays causing and not allowing for the measurement of light elements.

Matrix effect

When working with XRF, it is important to be aware of the effect the matrix has on samples. When samples containing multiple different similarly sized elements are measured, potential spectral overlap occurs (Gallhofer & Lottermoser, 2018). Furthermore, some compounds can absorb or scatter the characteristic X-rays from other elements causing those elements to be detected less. Some elements can be excited a second time from the characteristic X-rays of other elements in the matrix. This leads the second element to release more characteristic X-rays whilst absorbing the others. (Bruce Kaiser, 2008) For example, the K β_1 X-ray of Vanadium has an energy of 5,427.29 eV whilst the Chromium K α_1 has an energy of 5,414.72. When a sample containing both of these elements is excited, each element has a chance to absorb the X-rays of the other, causing interference and therefore errors in the measurement (Reichwein & Burgess, 2014).

Interference correction

There are several ways to correct for the matrix effect mentioned above. The first is measuring many samples of known concentrations and using statistical multiple linear regression analysis to determine the correction coefficient. This is a complex and time-consuming way to determine what the elemental interference is between two or more elements. Several theoretical algorithms have been proposed to calculate the interference using just the calibration curve. These equations calculate the theoretical influence of any element on the desired element. The simplest of these algorithms is the Lachance-Trail equation (Sitko & Zawisza, 2012). The equation is shown below.

$$W_i = R_i \left[1 + \sum_j \alpha_{ij} W_j \right]$$

Figure 5: Lachance-Trail algorithm for interelement correction (Sitko & Zawisza, 2012)

W_i = weight fraction of analyte
 R_i = relative intensity of analyte
 α_{ij} = the influence coefficient of element j on element i
 W_j = weight fraction interfering element

This equation considers the interference of all other components on the analyte. However, it does not correct for the effect of the analyte on itself.

$$W_i = E_i R_i \left[1 + \sum_{\substack{j \\ j \neq i}} \alpha_{ij} W_j \right]$$

Figure 6: De Jongh algorithm for interelement correction (Sitko & Zawisza, 2012)

W_i = weight fraction of analyte
 E_i = constant determined during calibration
 R_i = relative intensity of analyte
 α_{ij} = the influence coefficient of element j on element i
 W_j = weight fraction of interfering element

The de Jongh algorithm is a slightly more complex version of the first algorithm suited to multielement correction (Sitko & Zawisza, 2012). The de Jongh correction also determines the effect of the analyte on itself, as shown in figure 6 above. The result of using this equation is that the analyte intensity is adjusted such that the influence of all other compounds in the matrix is removed from this intensity, and an accurate representation of the analyte concentration is given.

Materials and Methods

Materials

Chemicals

All standards used in the calibration of the 26-element method were purchased from X-Ray Services in Belgium. The mineral oil used was purchased from Acros Organics. The dibutyl sulfide, barium 2-ethylhexanoate and bis(2-ethylhexyl) phosphorus were purchased from Sigma Aldrich. The calcium and zinc 2-ethylhexanoate were purchased from Alfa Aesar. The 10 μ m polypropylene, and 3.4 μ m/2.5 μ m Mylar foils were all purchased from Chemplex.

Methods

The temperature of the palladium source was set to 36.5°C and the flow of P10 gas was set to 24.7mL/min. When helium atmosphere was used, two different flows were set. The first was 10L/min and this was used when the system was being flushed after atmosphere change or when a sample entered or existed the sample chamber. During measuring or when the machine was in standby a helium flow of 500mL/min was used.

Prior to the analysis on any standard of sample, the atmosphere in the XRF was changed from vacuum to helium and allowed to stabilize for 30 minutes. To ensure that the apparatus is functioning, a pulse height adjustment is done each time the atmosphere is changed from vacuum to helium. This is done by measuring a sample provided by the manufacturer and ensures that the maximum intensity is being measured.

To validate the methods the limits of detection and quantification were determined by multiplying the standard deviation of blanc standards three and ten times respectively. Furthermore, repeatability was determined by measuring the same sample multiple times in one day and using the standard deviation of these results. Reproducibility was determined by calculating the standard deviation of the same sample being measured on different days and then multiplying this by $2\sqrt{2}$ to compensate for the fact that these results were obtained in one laboratory.

Sample vessels are prepared by stretching a foil membrane between two rings. The foil was laid across the area of the larger ring and the smaller ring was pressed into the foil and larger ring. The foil window was then checked for any surface deformation and rejected if this was present. These foil membranes often have trace elements on their surface which can be compensated for by using these for blank measurements and subsequently all measurements for the calibration and samples. It is paramount that these foils are of uniform thickness as deviations in foil thickness will cause variations in the results.

Method development

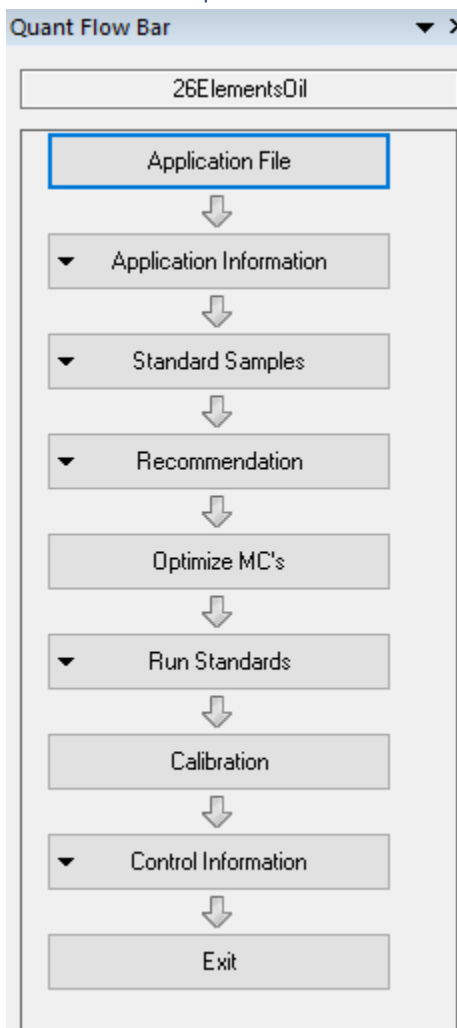


Figure 7: Steps taken to build an application file on the Supermini 200 software

Figure 7 shows the steps that need to be taken to make an application that can be used. In the first step, application information, the elements that were measured using the application were selected and the size of the sample vessel (34.7mm) as well as the weight of the sample (10.00g) were set.

In the standard samples tab, the concentrations of each analyte in the calibration is set. For multielement standards the concentration of each individual analyte was put in.

Under the tab recommendation the crystals as well as other measuring conditions are chosen.

El.line	Type	Target	kV-mA	Filter	Slit	Crystal	Detector	PHA
Mg-KA	Private	Pd	50-4.00	OUT	Std	RX26	PC	100- 260
Al-KA	Private	Pd	50-4.00	OUT	Std	RX26	PC	100- 260
Si-KA	Private	Pd	50-4.00	OUT	Std	RX26	PC	100- 300
P -KA	Private	Pd	50-4.00	OUT	Std	RX9	PC	100- 300
S -KA	Private	Pd	50-4.00	OUT	Std	RX9	PC	100- 300
Cl-KA	Private	Pd	50-4.00	OUT	Std	RX9	PC	100- 300
K -KA	Private	Pd	50-4.00	OUT	Std	RX9	PC	100- 300
Ca-KA	Private	Pd	50-4.00	OUT	Std	RX9	PC	100- 300
Ti-KA	Private	Pd	50-4.00	OUT	Std	LiF(200)	SC	100- 350
V -KA	Private	Pd	50-4.00	OUT	Std	LiF(200)	SC	100- 350
Cr-KA	Private	Pd	50-4.00	OUT	Std	LiF(200)	SC	100- 300
Mn-KA	Private	Pd	50-4.00	OUT	Std	LiF(200)	SC	100- 350
Fe-KA	Private	Pd	50-4.00	OUT	Std	LiF(200)	SC	100- 350
Co-KA	Private	Pd	50-4.00	OUT	Std	LiF(200)	SC	100- 350
Ni-KA	Private	Pd	50-4.00	OUT	Std	LiF(200)	SC	100- 350
Cu-KA	Private	Pd	50-4.00	OUT	Std	LiF(200)	SC	100- 340
Zn-KA	Private	Pd	50-4.00	OUT	Std	LiF(200)	SC	100- 320
Br-KA	Private	Pd	50-4.00	OUT	Std	LiF(200)	SC	100- 300
Mo-KA	Private	Pd	50-4.00	OUT	Std	LiF(200)	SC	100- 310
Ag-KA	Private	Pd	50-4.00	Zr...	Std	LiF(200)	SC	100- 300
Cd-KA	Private	Pd	50-4.00	Zr...	Std	LiF(200)	SC	100- 300
Sn-KA	Private	Pd	50-4.00	Zr...	Std	LiF(200)	SC	100- 300
Sb-KA	Private	Pd	50-4.00	Zr...	Std	LiF(200)	SC	100- 300
Ba-LA	Private	Pd	50-4.00	OUT	Std	LiF(200)	SC	100- 350

Figure 8: Measuring conditions for multielement method

Figure 8 shows an example of which measuring conditions were selected for various elements. Measuring time was set to be 40 seconds per element and 40 seconds for the background. The target (Pd) and the voltage/amperage (50-4.00) for all elements are the same as these are the settings of the source. As can be seen a filter option can be selected. This is the Zr filter that allows the palladium source lines to be absorbed so that these do not interfere with the measurement of these elements. Crystal selections were made to use the optimal crystals as suggested by Rigaku. The detector was selected with the PC being used for light elements up to and including calcium. The SC was used for all heavier elements. Lastly the PHA window was set to be between 100-300 unless interference was observed in which case the window was either extended to measure past the interference or reduced to not measure the interference.

In the tab Optimize MC's the measuring conditions were determined by measuring the fused beads to allow for determination of background angles as well as potential interference.

Figure 9: Optimization of measuring conditions

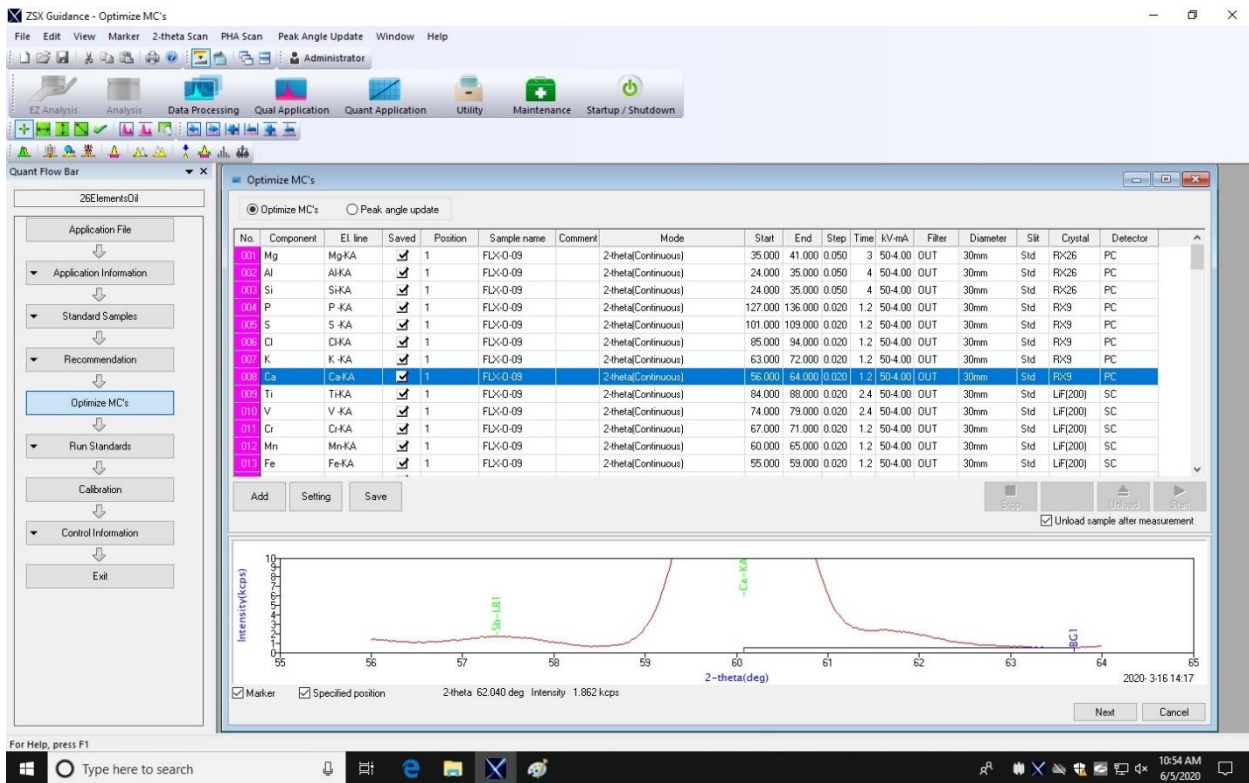


Figure 9 shows a scan to optimize the measuring conditions for calcium. In this example the background was set at a crystal angle of 63.75 degrees. This was done for each individual element as well as allowing to see if there was interference.

After optimizing the settings for each element, the standards were measured and calibrations were made. Once the elements were calibrated the results were corrected according to the de Jongh correction

algorithm.

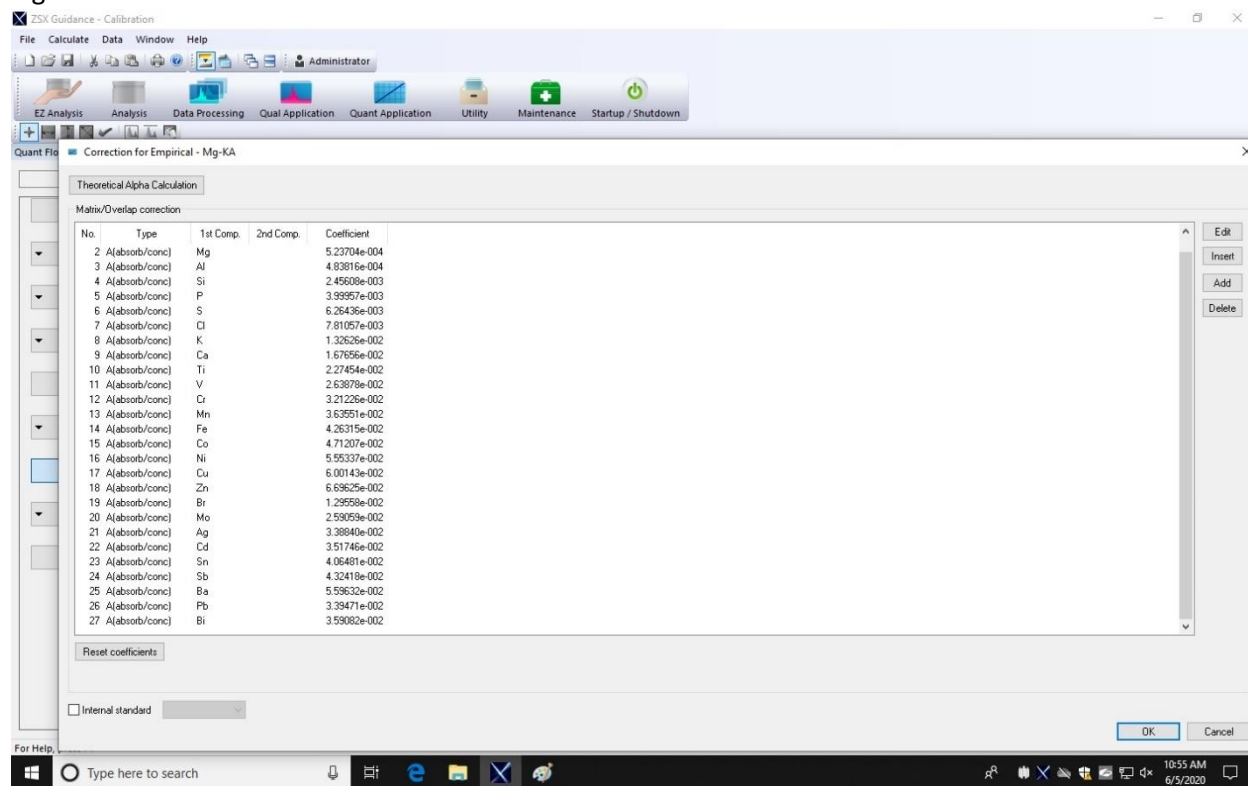


Figure 10: Values calculated according to the de Jongh algorithm for the correction of magnesium

Figure 10 shows an example of the values calculated by the de Jongh algorithm. As can be seen a correction value is calculated for each element on magnesium. This was repeated for every element to ensure that the calibrations were optimal and accurate to the standards.

Once this step was completed the method was linked to the beads used to optimize the measuring conditions so that when the calibrations begin to drift these can be corrected with a stable sample.

Multielement

Sample vessels were prepared using a 10 μ m polypropylene foil. Standards of each individual element as well as mixed standards were used to calibrate this method. Sample vessels were filled with 10.0 \pm 0.2g of standard or sample and subsequently measured. To ensure homogeneity among the samples each was shaken vigorously before measurement and allowed to sit to ensure all visible air bubbles have escaped from the samples. Viscous samples were heated to 50°C prior to homogenization. To calibrate the apparatus, first single element standards were measured to determine the crystal angle at which the highest intensity was measured. All elements up to antimony were measured using their K α X-rays whilst elements from antimony up are measured using their L α X-rays. Once optimized the apparatus was calibrated. Where interference was suspected the De Jongh correction algorithm was used to account for the matrix effect. Once calibrated the method was linked to fused beads containing all elements in question. These beads serve as drift control standards and will allow for the correction of each calibration.

ASTM D2622

The first standardized method is the ASTM D2622, which is used to determine the sulfur content in petroleum products. To calibrate this method three different sulfur ranges (0-0.1%, 0.1-1.0%, 1-5%) were made using dibutyl sulfide as a sulfur standard and mineral oil as a solvent. The optimal measuring angle was determined by measuring the highest standard of each line. A 3.6µm Mylar film was used to create the sample vessels.

The calibration was checked with external standards and these were used to determine the reproducibility and repeatability in the same manner as mentioned above and compared to the values calculated according to the methods shown below.

$$\text{Repeatability } (r) = 0.5006 \times x^{0.8015} \text{ ppm}$$

$$\text{Reproducibility } (R) = 1.4533 \times x^{0.8015} \text{ ppm}$$

Due to the fact that reproducibility is measured across different laboratories for this method, it was divided by $\sqrt{2}$ to compensate for the fact that the results obtained in this research come from the same laboratory and the same WD-XRF.

ISO 20884

Lastly, the sulfur content of automotive fuels was determined according to the ISO 20884 method. This method can accurately determine sulfur contents ranging from 5ppm to 500ppm in fuels containing no more than 3.7% oxygen. Two external calibration ranges (0-50ppm, 0-500ppm) were prepared by diluting dibutyl sulfide in mineral oil. A Mylar film of 2.5µm was used for sample vessels. The Supermini200 has a source with lower power than stated in the method and therefore to conform to the method the measuring time was set such that the counts obtained from the 50ppm standard were above 50,000. The repeatability and reproducibility were compared to those calculated conform to the method. These calculations are below.

For the calibration range of 0-50ppm

$$\text{Repeatability } (r) = 1.7 + 0.0248x \text{ ppm}$$

$$\text{Reproducibility } (R) = 1.9 + 0.1201x \text{ ppm}$$

For the calibration range of 50-500ppm

$$\text{Repeatability } (r) = 4 \text{ ppm}$$

$$\text{Reproducibility } (R) = 4.6 + 0.075x \text{ ppm}$$

In this method the reproducibility was also be divided by $\sqrt{2}$ to compensate for the fact it was measured in one laboratory on the same WD-XRF.

Results and Discussion

Each time the atmosphere was changed from vacuum to helium a pulse height adjustment (PHA) was done. To do this the standard sample provided by Rigaku was measured under the same conditions. The results of all are shown below.

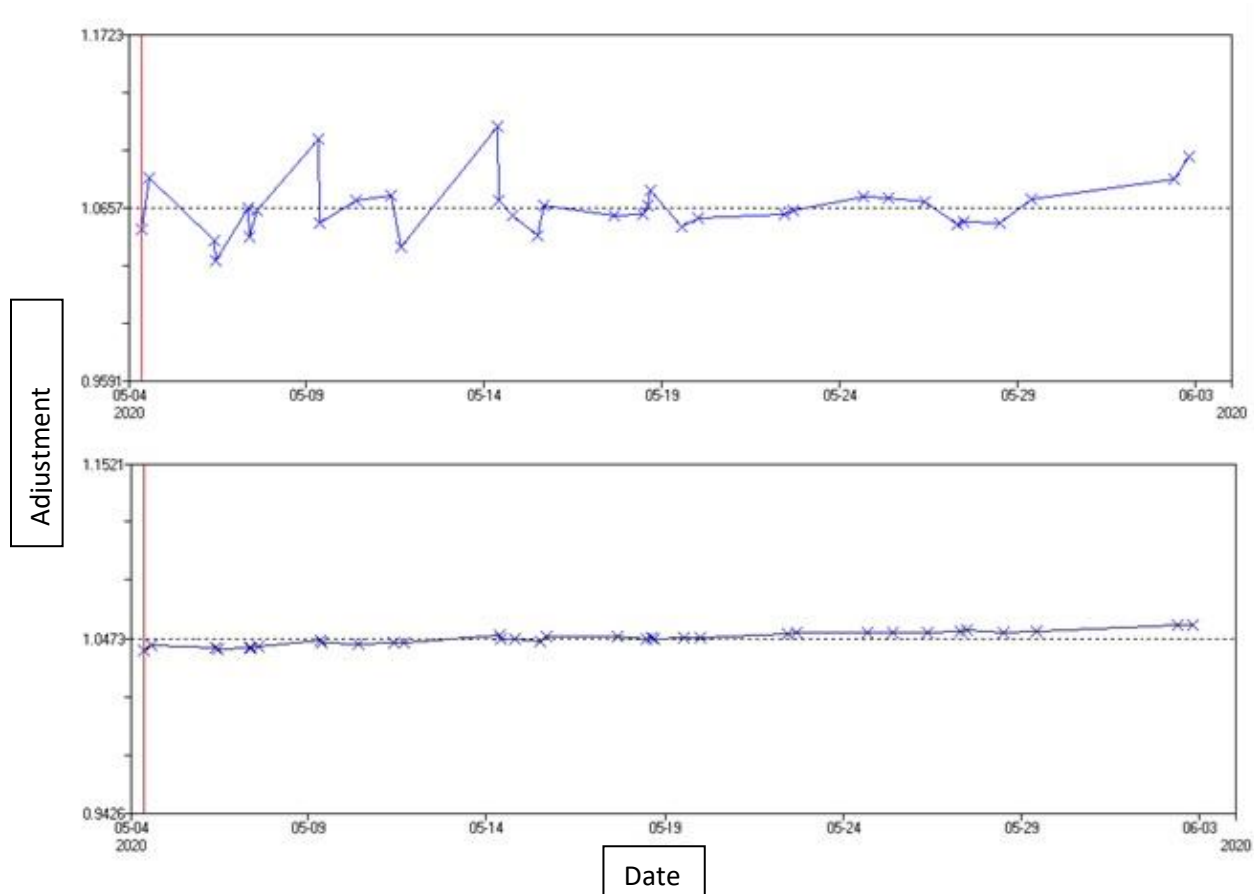


Figure 11: PHA values taken across 1 month (top PHA values of proportional counter, bottom PHA values of scintillation counter)

Figure 5 shows that over time there is only slight variation to the value of the PHA. The top graph shows the results of the PHA on the proportional counter. As can be seen on this graph there are some relatively large increases in the PHA values followed by drop. These high values were obtained when the PHA was carried out immediately after atmosphere change. This suggests that the atmosphere in the apparatus had not yet fully stabilized and when measured sometime later the values return to “normal”. It can also be seen that the stabilization has little effect on the scintillation counter as indicated by the flatness of the bottom graph. Furthermore, both graphs show an upward trend increasing slowly overtime. This drift is caused by the aging of the X-ray source as it is continuously on. The figure shows that over a month the value for the PHA increases slightly. This being said, it is not necessary to measure this value everyday as it does not vary enough to warrant daily checks.

Multielement method

When magnesium was calibrated on the apparatus the results varied from one measurement to the next. It was noted that at the same time 8 helium tanks had been used in two days. It was suspected that there

was a leak somewhere in the Supermini 200. To test this a separate tank of helium was attached to the machine and it left under helium atmosphere for several days. During this time a record was kept of the pressure inside the tank. A tank of helium contains 10,000 liters of helium. At a flow rate of 0.5L/min the tank was calculated to last almost 14 days. At the end of the week the pressure in the tank had halved suggesting that the leak was not in the Supermini 200. As a result of this when the tank was almost empty it was removed, and the apparatus was reattached to the gas system.

All calibrations done for the multielement method were corrected for interference and corrected such that the correlation coefficient of each regression was 0.9999 or higher. An example of this interference is shown below.

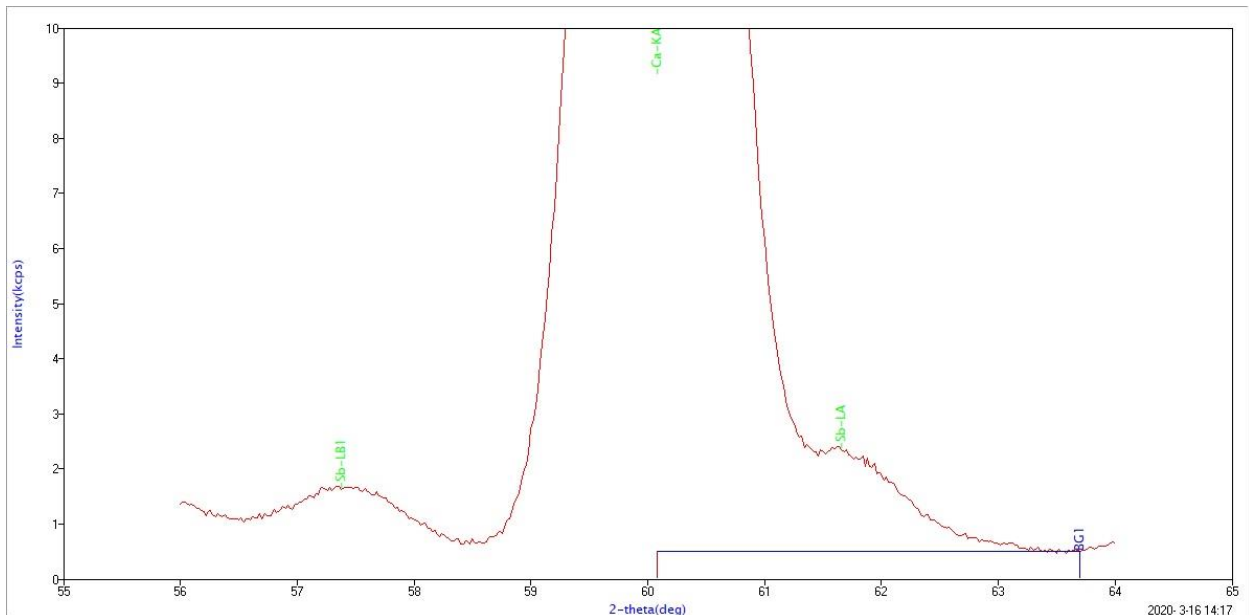


Figure 12: Scan of optimal crystal angle for the measurement of calcium $K\alpha$ together with background measurement

Figure 6 shows a scan made to determine the optimal angle of the diffraction crystal to measure the $K\alpha$ X-ray of calcium. It can be seen that along with a large signal for calcium there are two smaller signals present of $L\alpha/\beta$ lines of antimony. The first of which having no effect on the intensity measured. However, the second peak is partially interfering with the calcium signal. This suggests that there is a slight spectral overlap between the antimony $L\alpha$ and calcium $K\alpha$ X-ray intensities. Due to this being a standard the concentration of both elements is known and the de Jongh correction was used to calculate a theoretical coefficient for this interference which in future measurements will be used to subtract the antimony $L\alpha$ intensity from that of the calcium $K\alpha$. In this case the background is measured at one point indicated by BG1 on the figure. The figure also shows why it is not possible to measure the background on both sides of peak. The $Sb-L-\beta_1$ peak makes it so that the signal does not return to the baseline. If the second background measurement would be made at approximately 58.5 then this would lead to a change in peak maxima.

Table 1: LoD and LoQ data for elements Mg-Ca

Element	RX26			RX9				
	Mg	Al	Si	P	S	Cl	K	Ca
Measurements	12	12	12	12	12	12	12	12
Average	-1.31	0.02	3.42	0.22	0.15	1.05	-3.13	-0.32
Maximum	14.7	13.0	15.5	0.7	1.9	3.0	-0.8	0.9
Minimum	-21.7	-12.0	-8.3	-0.4	-0.6	0.2	-6.0	-1.5
Std dev.	11.4	7.1	5.8	0.4	0.5	0.7	1.6	0.7
LoD	34.2	21.4	17.3	1.2	1.6	2.0	4.8	2.2
LoQ	113.9	71.3	57.5	3.9	5.4	6.6	16.0	7.3

As can be seen in table 1 the LoD and LoQ decrease as the size of the atom increases. This is due to the fact that light elements emit X-rays with low energies. These low energy X-rays are absorbed easily by the matrix, foil and atmosphere in the detector. Furthermore, the fact that they cannot penetrate through the matrix means these elements are only measured in the first few micrometers of the sample resulting in low intensities being observed.

Table 2: LoD and LoQ data of elements Ti-Bi

Element	LiF200																	
	Ti	V	Cr	Mn	Fe	Co	Ni	Cu	Zn	Br	Mo	Ag	Cd	Sn	Sb	Ba	Pb	Bi
Measurements	12.0	12.0	12.0	12.0	12.0	12.0	12.0	12.0	12.0	12.0	12.0	12.0	12.0	12.0	12.0	12.0	12.0	12.0
Average	1.4	-0.4	0.4	0.2	-0.2	-0.4	0.1	-0.4	0.2	-0.1	0.8	-0.7	-0.2	6.8	6.7	0.2	-0.2	1.0
Maximum	2.2	0.6	1.6	1.9	0.8	0.7	0.9	0.2	0.9	0.7	2.3	4.2	7.2	13.7	19.5	5.5	1.9	3.1
Minimum	0.0	-1.6	-0.6	-1.2	-1.5	-1.2	-0.7	-1.2	-0.5	-1.1	-0.2	-7.1	-3.6	-1.4	-9.4	-3.7	-1.4	-0.7
Std dev.	0.8	0.7	0.6	1.0	0.7	0.5	0.5	0.4	0.4	0.6	0.8	3.0	3.2	4.5	8.8	3.4	1.0	1.3
LoD	2.5	2.2	1.9	2.9	2.1	1.5	1.5	1.2	1.2	1.7	2.4	8.9	9.7	13.6	26.5	10.2	3.1	3.8
LoQ	8.2	7.3	6.3	9.6	6.9	5.1	5.0	4.1	4.1	5.8	8.0	29.7	32.2	45.3	88.2	34.0	10.3	12.8

Table 2 shows a trend where the standard deviation increases and then decreases again between molybdenum and bismuth. From antimony to bismuth the $L\alpha$ lines are used to measure the element because the $K\alpha$ lines are subject to spectral overlap from several different elements. This makes it hard to correct for the interference as there are too many variables. This results in a drop in intensity for these elements which subsequently leads to higher variability between measurements. The table also shows that from molybdenum to tin the LoD and LoQ are rising. This is due to the fact that these elements are subject to increasing amounts of spectral interference as some lighter elements emit their $L\alpha$ lines in these regions. These elements are still measured using their $K\alpha$ X-rays because the intensities of the $L\alpha$ X-rays are too low and will result in higher variation.

Reproducibility was determined by measuring a mixed standard of 10ppm containing 20 of the 26 elements measured in this method across several days and looking at the standard deviation of each measurement.

Table 3: Reproducibility data of 10 elements, of light to medium mass at a concentration of 10 ppm, measured according to the multielement method

Element	Mg	Al	Si	P	K	Ca	Ti	V	Cr	Mn
	ppm									
Maximum	22	18	23	10	10	10	12	13	11	12
Minimum	1	3	6	9	4	8	11	9	10	11
Average	15	11	12	10	7	9	11	11	10	11
Std dev.	7	6	6	1	2	1	0	1	1	0
RSD(%)	51	59	46	5	26	6	4	9	5	4

Table 3 shows that the reproducibility of the method increases with the mass of the element. Due to the low intensity obtained when measuring light elements there is high variation among measurements as indicated by the minimum and maximum measurements for elements such as magnesium and aluminum. The variation is such that when measuring these light elements at a concentration of 10ppm there is a chance that they are detected at double the concentration of at almost 0. As mentioned before this could be due to variations in the foil thickness as well inhomogeneity of the sample.

Table 4: Reproducibility data of 10 elements, of medium to high mass at a concentration of 10 ppm, measured according to the multielement method

Element	Fe	Ni	Cu	Zn	Mo	Ag	Cd	Sn	Ba	Pb
	ppm									
Maximum	11	11	10	11	12	15	18	20	18	10
Minimum	9	10	9	10	9	9	7	2	3	5
Average	10	10	10	11	11	12	11	13	14	8
Std dev.	1	0	1	0	1	2	4	6	5	2
RSD(%)	6	4	5	2	10	19	34	49	36	26

Table 4 shows that the heavier elements are measured with less variation as they are less susceptible to small differences in foil thickness, contamination or inhomogeneity. This being said it can be seen that similarly to the LoD and LoQ the values increase for elements silver to tin and then decrease for barium and lead. The reason for this increase is the same as previously stated namely that silver to tin have increased interference from the $L\alpha/\beta$ lines of lighter elements. These elements however lack the intensity on their $L\alpha/\beta$ lines to be measurable. When measuring the heaviest elements like barium and lead with the $L\alpha$ lines the interference decreases and the reproducibility decreases as well.

ASTM D 2622

When calibrating this method, it was noticed that as concentrations became higher the linearity of the calibrations changed. This was most apparent in the calibration range from 1-5% sulfur. The figure below shows the calibration curve attained.

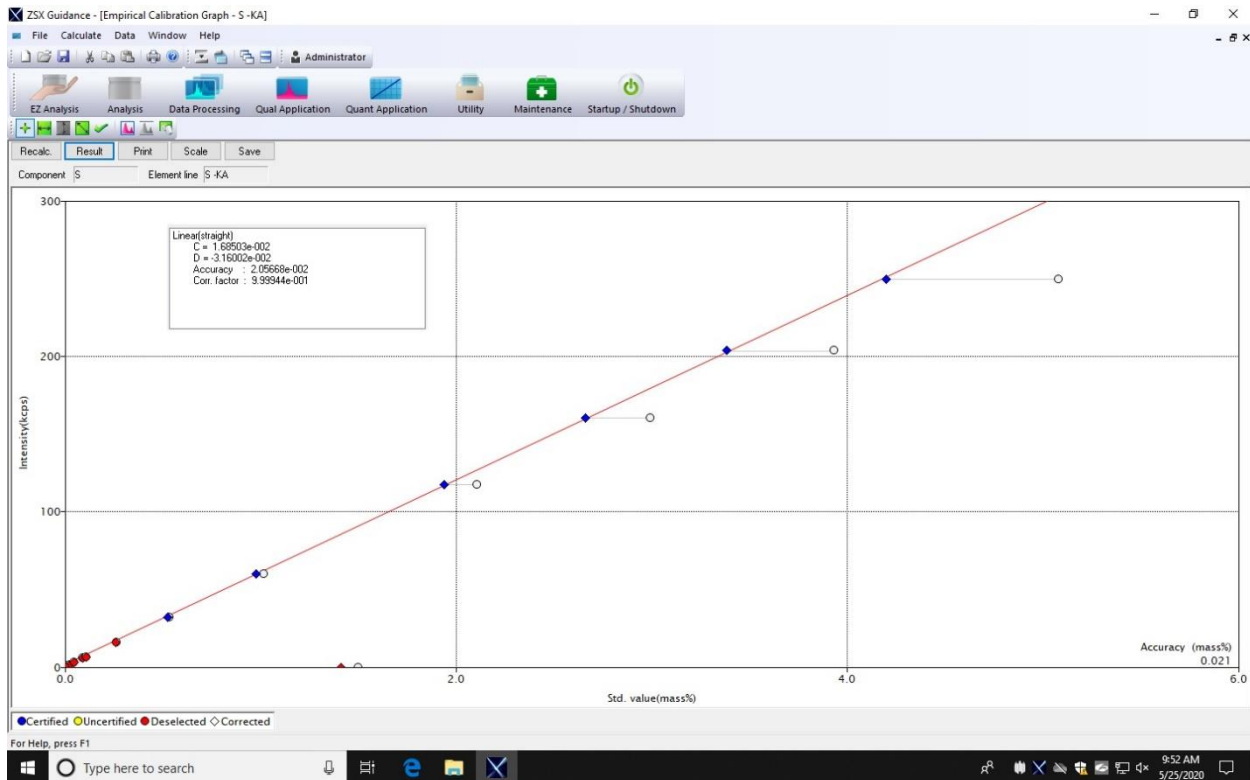


Figure 13: The optimized calibration of sulfur from 1-5% by mass according to the ASTM D 2622

Figure 6 shows the calibration line for high sulfur standards according to ASTM D 2622. The points in white indicate the original measured standards from which the calibration is made. As can be seen the intensities start to flatten out suggesting that the measurements being done are outside of the linear range for this machine. The blue points are corrected for the matrix effect according to the de Jongh algorithm. The amount of correction present at each point increases substantially. This is due to the fact that there are more sulfur atoms to interfere with and scatter the emitted X-rays of other sulfur atoms.

The LoD and LoQ for this method were found to be 1.8 and 6.0ppm respectively. The lower limit of samples measured on the low sulfur line is 10ppm meaning that samples can be accurately reported as being below the spec. When comparing these results to the multielement method they have similar values.

Table 5: Validation results for the determination of sulfur in petroleum products according to ASTM D2622

Calibration range	Repeatability mass% (calculated)	Repeatability mass% (method)	Reproducibility mass% (calculated)	Reproducibility mass% (method)
Low (0-0.1%)	6.0×10^{-5}	1.1×10^{-4}	1.4×10^{-4}	1.9×10^{-4}
Medium (0.1-1.0%)	0.013	0.013	0.012	0.037
High (1.0-5.0%)	0.018	0.071	0.129	0.146

Table 3 shows the results of the validation of each calibration line. As can be seen in the table the repeatability and reproducibility of all calibration lines are lower than that specified in the method.

ASTM D4927

Two of the standards, namely the barium 2-ethylhexanoate and the calcium 2-ethylhexanoate, proved to be insoluble in mineral oil even when heated to 40°C in an ultrasonic bath. To allow for calibration it was attempted to dissolve these compounds in small volumes of other organic solvents which could then be dissolved in mineral oil. According to the method xylene could be used to dissolve these standards but when attempted the calcium 2-ethylhexanoate would not dissolve. It was noted that out of the two standards the calcium 2-ethylhexanoate was the hardest to dissolve and was therefore used for subsequent trials. Heptane, tetrahydrofuran (THF), carbon disulfide (CS₂) and ethanol were chosen. These were chosen because they range from nonpolar to polar and are known to be strong solvents. The calcium standard proved to be soluble in polar solvents like ethanol and THF and not in nonpolar solvents like heptane or CS₂.

It was decided to continue using ethanol as a solvent because it is less reactive and less dangerous than THF. Before trying to make a standard the miscibility of ethanol and mineral oil was tested. It was found out that ethanol is not miscible with mineral oil because it is too polar. To reduce the polarity of the solvent it was decided to use a longer chain alcohol. After testing propanol, hexanol and octanol it was found that hexanol provided the best miscibility with mineral oil whilst still dissolving all the standard.

Before calibration a standard was made according to the method using hexanol to make the stock solution for barium and calcium and then further diluting that with mineral oil. To ensure the quality of the standard it was measured using inductively coupled plasma atomic emission spectroscopy (ICP-AES) to determine whether all the standard had dissolved properly. However, when the standard was measured using ICP-AES it was found that the concentrations were lower than theoretically calculated. Furthermore, an analysis of the sample using the 26-element method yield similar low results as well as showing that the Mylar film used to make the sample vessel showed significant degradation. Once it was found that the matrix affected the foil and risk rupturing the foil during measurements it was decided to order the standards again from a different supplier.

ISO 20884

This method mentions that the WD-XRF apparatus should produce a voltage no less than 30kV and a current of no less than 50mA. The Rigaku Supermini200 has a maximum voltage of 50kV however it can only produce up to 8mA. To correct for this the method suggests that if a system does not have the required power then it can be optimized such that the total counts for a 50ppm standard are equal to or greater than 40,000. To ensure that the measurements done conform the method a measuring time of 300 seconds was chosen leading to a total count of 120,000 for the 50ppm standard.

The limit of detection was determined by measuring 8 blanks and is calculated to be 0.9 ppm whilst the limit of quantification is 3ppm. This is significantly lower than that of the previous methods. This is due to the foil used in the sample vessel preparation. The film used is much thinner (2.5µm) than the other methods allowing more emitted X-rays to pass through the sample. Though this foil allows for lower measurements it comes with risks. This foil is very susceptible to damage when a sample vessel is made. To ensure that no damaged vessels are measured a leak check was done before each measurement to ensure that no sample would spill onto the X-ray source.

Table 6: Validation results for the determination of sulfur in automotive fuels according to ISO 20884

Calibration range	Repeatability _{ppm} (calculated)	Repeatability _{ppm} (method)	Reproducibility _{ppm} (calculated)	Reproducibility _{ppm} (method)
Low (0-50ppm)	0.40	1.9	1.98	2.11
High (50-500ppm)	0.8	4.0	5.4	22

Table 4 shows that the validation results obtained are conform the method. These results are significantly lower than those in the method suggesting that the Supermini 200 is more precise and accurate when measuring sulfur in automotive fuels.

Conclusion

The calibration of a multielement method which measures 26 different elements was achieved using the de Jongh correction algorithm as well as the optimized measuring conditions determined by scanning each element for optimal crystal angle as well as potential interference. With this the LoD and LoQ were determined for all elements and the method could be used on samples. The reproducibility was determined for 20 elements and shows similar results to that of their LoD and LoQ. Furthermore, the standardized methods ASTM D2622 and ISO 20884 were calibrated and validated and found to be more precise than that of the method that was used even after correction for the interlaboratory effect. The calibration of ASTM D4927 was attempted and not successful. The standards were insoluble in the matrices stated in the method however proved soluble in polar solvents. The calibration was attempted again but once it was noticed that the polar solvents degraded the foil used to make the sample vessels the method was abandoned until new standards arrive. Lastly, it was shown that helium use could be reduced by measuring the PHA chip less frequently.

Recommendations

Firstly, the repeatability of the multielement method should be determined and round robin samples should be measured to see if the reproducibility of this method is close to that of the round robin. Secondly, there are many more methods both standardized and not that can be applied to the Rigaku Supermini200. Once new standards arrive the calibration of the ASTM D4927 should be attempted again. Furthermore, the multielement method only contains 26 elements and it could potentially be expanded to measure more elements. The effect of the de Jongh correction algorithm should be determined more accurately by looking at what the actual difference between this algorithm and the Lachance algorithm are in practice. The effect of stabilization time, after atmosphere changes, on measurements should be investigated to determine whether it is possible to shorten the duration of stabilization prior to measuring. This along with investigating the frequency at which the pulse height adjustments should be done could significantly decrease the measurement times for analysts and with it the helium use of the Supermini 200.

Bibliography

- Agency for Toxic Substances and Disease Registry. (1999, June). *Sulfur Dioxide*. Retrieved from ATSDR.cdc.gov:
<https://www.atsdr.cdc.gov/toxfaqs/tfacts116.pdf?fbclid=IwAR1cWrhtgr8AVaEvgO5vVq2VALtTY Sb7-NnvYV0tt7zsrB0ApvrYt9SapyU>
- Bertin, E. P. (1978). *Principles and Practice of X-ray spectrometric Analysis*. New York: Plenum Press.
- Brouwer, P. (2003). *Theory of XRF*. Almelo: PANalytical B.V.
- Bruce Kaiser, A. W. (2008). *BRUKER XRF SPECTROSCOPY USER GUIDE*. Bruker.
- Bruker AXS. (2000). *Introduction to X-ray Fluorescence*. Karlsruhe: Bruker AXS.
- Chatterjee, A. K. (2001, December 16). X-Ray Diffraction. *Handbook of Analytical Techniques in Concrete Science and Technology*, pp. 275-332.
- Gallhofer, D., & Lottermoser, B. G. (2018). The Influence of Spectral Interferences on Critical Element Determination with Portable X-Ray Fluorescence (pXRF). *Minerals*.
- Kramar, U. (1999, June 17). X-Ray Fluorescence Spectrometers. *Encyclopedia of Spectroscopy and Spectrometry*, pp. 2467-2477.
- Potts, P. J. (2005). X-RAY FLUORESCENCE AND EMISSION | Wavelength Dispersive X-Ray Fluorescence. *Encyclopedia of Analytical Science (Second Edition)*, 419-429.
- Reichwein, E., & Burgess, B. (2014). *X-ray Fluorescence*. Santa Cruz: Department of Physics University of California, Santa Cruz.
- Simon R. Cherry, J. A. (2012, April 15). Interaction of Radiation with Matter. *Physics in Nuclear Medicine (Fourth Edition)*, pp. 63-85.
- Sitko, R., & Zawisza, B. (2012). *Quantification in X-Ray Fluorescence Spectrometry*. doi:10.5772/29367
- U.S. Energy Information Administration. (2019). *The Effects of Changes to Marine*. Washington DC: U.S. Energy Information Administration.

Appendix

I.

Bragg's law

$$n\lambda = 2d \sin \theta$$

II, Validation ASTM D2622

Herhaalbaarheid				S	CH2
				mass%	mass%
Zwavel	2622		4/8/2020		
Low		Repeatability 1	12:20	0.0013	99.999
Zwavel	2622		4/8/2020		
Low		Repeatability 2	12:27	0.0011	99.999
Zwavel	2622		4/8/2020		
Low		Repeatability 3	12:34	0.0012	99.999
Zwavel	2622		4/8/2020		
Low		Repeatability 4	12:41	0.0012	99.999
Zwavel	2622		4/8/2020		
Low		Repeatability 5	12:48	0.0012	99.999
Zwavel	2622		4/8/2020		
Low		Repeatability 6	12:55	0.0012	99.999
Zwavel	2622		4/8/2020		
Low		Repeatability 7	13:02	0.0013	99.999
Zwavel	2622		4/8/2020		
Low		Repeatability 8	13:09	0.0012	99.999
Number				8	8
Average				0.0012	99.999
Maximum				0.0013	99.999
Minimum				0.0011	99.999
Range				0.0002	0
Std dev.				0.00006	0.0001
RSD(%)				4.76	0
herhaalbaarheid methode				0.000107	

Reproduceerbaarheid

				S	CH2
				mass%	mass%
Zwavel	2622		4/15/2020		
Low		qc 10ppm check	14:47	0.001	99.999
Zwavel	2622		4/16/2020		
Low		Qc low	14:48	0.0009	99.999
Zwavel	2622		4/17/2020		
Low		qc low	12:31	0.001	99.999
Zwavel	2622		4/20/2020		
Low		qc low	9:46	0.001	99.999

Zwavel	2622			4/21/2020		
Low		qc		14:24	0.001	99.999
Zwavel	2622			4/22/2020		
Low		qc		11:32	0.001	99.999
Zwavel	2622			4/24/2020		
Low		qc		10:20	0.0011	99.999
Zwavel	2622			4/28/2020		
Low		qc		12:14	0.001	99.999
Zwavel	2622			4/29/2020		
Low		qc		10:45	0.001	99.999
Zwavel	2622			4/30/2020		
Low		QC	RvT	11:48	0.001	99.999
Number					10	10
Average					0.001	99.999
Maximum					0.0011	99.999
Minimum					0.0009	99.999
Range					0.0002	0
Std dev.					0.00005	0
RSD(%)					4.77	0
Repro methode					0.000271	
Repro lab					0.000191	
Repro gemeten					0.000141	

LoD, LoQ

				S	CH2
				ppm	mass%
Zwavel	2622	Blanco	4/6/2020		
Low		1	10:37	3	100
Zwavel	2622	Blanco	4/6/2020		
Low		2	10:44	2	100
Zwavel	2622	Blanco	4/6/2020		
Low		3	10:51	0	100
Zwavel	2622	Blanco	4/6/2020		
Low		4	10:58	1	100
Zwavel	2622	Blanco	4/6/2020		
Low		5	11:05	1	100
Zwavel	2622	Blanco	4/6/2020		
Low		6	11:12	1	100
Zwavel	2622	Blanco	4/6/2020		
Low		7	11:20	1	100
Zwavel	2622	Blanco	4/6/2020		
Low		8	11:27	1	100
Zwavel	2622	Blanco	4/6/2020		
Low		9	11:34	0	100

Zwavel	2622	Blanco	4/6/2020		
Low		10	11:41	1	100
Zwavel	2622	Blanco	4/6/2020		
Low		11	11:48	1	100
Zwavel	2622	Blanco	4/6/2020		
Low		12	12:02	0	100
Number				12	12
Average				1	100
Maximum				2	100
Minimum				0	100
Range				2	0
Std dev.				0.603023	0.0001
RSD(%)				89.95	0
LoD				1.809068	
LoQ				6.030227	

III, Validation ISO 20884

Herhaalbaarheid

				S	CH2
				mass%	mass%
S	ISO		4/22/2020		
20884L	Repeat low		14:34	0.001	99.999
S	ISO		4/22/2020		
20884L	Repeat low		14:41	0.001	99.999
S	ISO		4/22/2020		
20884L	Repeat low		14:48	0.001	99.999
S	ISO		4/22/2020		
20884L	Repeat low		14:55	0.0009	99.999
S	ISO		4/22/2020		
20884L	Repeat low		15:02	0.0009	99.999
S	ISO		4/22/2020		
20884L	Repeat low		15:09	0.0009	99.999
S	ISO		4/22/2020		
20884L	Repeat low		15:16	0.0008	99.999
S	ISO		4/22/2020		
20884L	Repeat low		15:23	0.0009	99.999
Number				8	8
Average				9	99.999
Maximum				0.001	99.999
Minimum				0.0008	99.999
Range				0.0001	0
Std dev.				0.4	0
RSD(%)				4.46	0
Herhaalheid methode				1.9232	

Reproduceerbaarheid

				S	CH2
				mass%	mass%
S	ISO	Repro	4/22/2020		
20884L	1		14:11	0.0009	99.999
S	ISO	Repro	4/23/2020		
20884L	2		15:25	0.0011	99.999
S	ISO	repro	4/28/2020		
20884L	4		12:38	0.0009	99.999
S	ISO	repro	4/29/2020		
20884L	5		16:14	0.001	99.999
S	ISO	repro	4/30/2020		
20884L	6		11:09	0.0008	99.999
S	ISO	repro	5/1/2020		
20884L	7		11:03	0.0009	99.999
S	ISO	repro	5/7/2020		
20884L	7	LV	12:52	0.0009	99.999
S	ISO	repro	5/8/2020 9:59		
20884L	8	LV		0.0009	99.999
Number				8	8
Average				9	99.999
Maximum				0.0011	99.999
Minimum				0.0008	99.999
Range				0.0002	0
Std dev.				0.7	0.0001
RSD(%)				7.2	0
Repro methode				2.9809	
repro					
lab				2.107815	
repro gemeten				1.979899	

LoD, LoQ

				S	CH2
				ppm	mass%
S	ISO		5/14/2020		
20884L	LOD	RvT	10:56	-1.00000	100
S	ISO		5/14/2020		
20884L	LOD	RvT	11:07	0.00000	100
S	ISO		5/14/2020		
20884L	LOD	RvT	11:18	0.00000	100
S	ISO		5/14/2020		
20884L	LOD	RvT	11:29	0.00000	100
S	ISO		5/14/2020		
20884L	LOD	RvT	11:41	0.00000	100
S	ISO		5/14/2020		
20884L	LOD	RvT	11:52	0.00000	100

	S	ISO		5/14/2020		
	20884L	LOD	RvT	12:03	0.00000	100
	S	ISO		5/14/2020		
	20884L	LOD	RvT	12:14	0.00000	100
Number					8	8
Average					0	100
Maximum					0	100
Minimum					-0.0001	100
Range					0.0001	0
Std dev.					0.3	0
RSD(%)					-100.4	0
LoD					0.9	
LoQ					3	

Herhaalbaarheid

	S	ISO		4/22/2020		
	20884H	Repeat high		15:37	0.0353	99.965
	S	ISO		4/22/2020		
	20884H	Repeat high		15:44	0.0352	99.965
	S	ISO		4/22/2020		
	20884H	Repeat high		15:51	0.0353	99.965
	S	ISO		4/22/2020		
	20884H	Repeat high		15:58	0.0353	99.965
	S	ISO		4/22/2020		
	20884H	Repeat high		16:05	0.0355	99.965
	S	ISO		4/22/2020		
	20884H	Repeat high		16:12	0.0353	99.965
	S	ISO		4/22/2020		
	20884H	Repeat high		16:19	0.0354	99.965
	S	ISO		4/22/2020		
	20884H	Repeat high		16:26	0.0354	99.965
Number					8	8
Average					353	99.965
Maximum					0.0355	99.965
Minimum					0.0352	99.965
Range					0.0002	0
Std dev.					0.8	0.0001
RSD(%)					0.21	0
Herhaalbaarheid methode					4	

Reproduceerbaarheid

S	CH2
mass%	mass%

S	ISO	Repro	4/22/2020		
20884H	1		14:18	0.0353	99.965
S	ISO	Repro	4/23/2020		
20884H	2		15:32	0.0355	99.965
S	ISO		4/24/2020		
20884H	qc 353 (LV)		10:58	0.035	99.965
S	ISO	repro	4/28/2020		
20884H	4		12:45	0.0352	99.965
S	ISO	repro	4/29/2020		
20884H	5		16:21	0.0349	99.965
S	ISO	repro	4/30/2020		
20884H	6		11:16	0.035	99.965
S	ISO	repro	5/1/2020		
20884H	7		11:10	0.0349	99.965
S	ISO	repro	5/8/2020		
20884H	8	LV	10:10	0.0352	99.965
Number				8	8
Average				351	99.965
Maximum				0.0355	99.965
Minimum				0.0349	99.965
Range				0.0005	0.001
Std dev.				1.9	0.0002
RSD(%)				0.54	0
Repro methode				30.925	
repro					
lab				21.86728	
repro gemeten				5.374012	